Extreme Mechanics Letters 46 (2021) 101347

Contents lists available at ScienceDirect

Extreme Mechanics Letters

journal homepage: www.elsevier.com/locate/eml

Self-adaptive acoustic cloak enabled by soft mechanical metamaterials

Yahui Xue [a], Xiang Zhang [a,b,*]

[a] Nanoscale Science and Engineering Center, University of California, Berkeley, CA, USA
[b] Faculty of Science and Faculty of Engineering, University of Hong Kong, Hong Kong, China

ARTICLE INFO

Article history:
Received 5 February 2021
Received in revised form 20 April 2021
Accepted 26 April 2021
Available online 1 May 2021

Keywords:
Acoustic cloak
Mechanical metamaterials
Negative Poisson's ratio

ABSTRACT

Acoustic cloaks enable exciting object concealment by manipulating sound waves and have attracted research efforts from different approaches such as transformation acoustics. However, the challenge still lies in the practical implementation of those cloaks that require complex material designs. Here, we show that an underwater acoustic cloak can be automatically achieved by deforming a soft mechanical metamaterial with Poisson's ratio of -1. The deformation of such an auxetic structure is demonstrated to be able to automatically and passively fulfill the requirement of quasi-conformal mapping for cloak design. Such a self-adaptive acoustic cloak exhibits a wide frequency and angular bandwidth, which opens an avenue for convenient design of various kinds of acoustic metamaterials.

Acoustic metamaterials enable the manipulation of sound waves in an unprecedented way and can realize intriguing functions ranging from subwavelength acoustic imaging to acoustic cloaking [1–3]. Coordinate transformation has been widely used to design acoustic cloaks to elaborately control the wave propagation paths based on the form invariance of wave equations [4]. However, it usually leads to the distortion of constitutive parameters in the medium to a high degree of anisotropy and inhomogeneity that greatly limits the choice of suitable materials [5]. Artificial structures with resonant components are able to generate desired dynamic material properties such as effective density and bulk modulus, which, instead, reduces the applicable frequency range and could also cause significant dissipation loss [6,7]. On the other hand, carpet cloaking, by concealing objects on a planar surface, has been proposed to simplify the design by loosening the requirement of material anisotropy or inhomogeneity. For example, based on the quasi-conformal mapping, a carpet cloak has been designed using inhomogeneous but isotropic materials [8,9]. Moreover, a linear coordinate transformation enables the construction of carpet cloaks using anisotropic but homogeneous structure components [10,11]. Nevertheless, the complexity of material design in a spatially varying manner still limits the utility of those cloaks.

Recently, soft mechanical metamaterials have attracted much attention for active wave control using reconfigurable structure design [12]. The deformation of those metamaterials naturally leads to the modulation of constitutive parameters in the medium that affects the wave propagation [13–17]. More interestingly, it is even possible to elaborately control the wave propagation paths by designing the deformation pattern of those mechanical metamaterials so as to acquire desired material property distribution [18]. The attempt has been also made in optics to design optical cloaks by deforming auxetic structures, which is shown to be able to meet the conditions of quasi-conformal mapping using matrix materials of ultrahigh permeability [19,20]. However, such exploration in acoustics still remain elusive due to the limited availability of suitable materials for transformation acoustics.

Here, we report a self-adaptive acoustic cloak automatically formed by elastically deforming a soft mechanical metamaterial in water, which shows broadband frequency and angular response. The matrix of the metamaterial is based on soft materials like silicone elastomer (or PDMS), which has the advantage to be feasibly adjusted to match the acoustic impedance of water [21]. The additional use of lattice structures with extreme mechanical property of Poisson's ratio equal to -1 makes its deformation spontaneously fulfill the requirement of quasi-conformal mapping. Such a mapping needs the effective sound speed variation follows a square-root relation with the volume change of the lattice cell. This can be obtained by introducing a second component (e.g., air) in the matrix to effectively tune the material acoustic property in a fraction average manner.

In order to obtain a self-adaptive acoustic metamaterial enabled by direct structure deformation, for simplicity, we inspect the requirement of 2D quasi-conformal mapping that has been commonly used to design carpet cloaks. This kind of mapping only needs the spatial distribution of isotropic materials. This provides the prerequisite for the structure deformation to realize such a design, that is, to maintain the material isotropy even after deformation. On the other hand, the density (ρ) and bulk modulus (κ) in the physical space due to the coordinate transformation

* Corresponding author.
E-mail address: president@hku.hk (X. Zhang).

https://doi.org/10.1016/j.eml.2021.101347

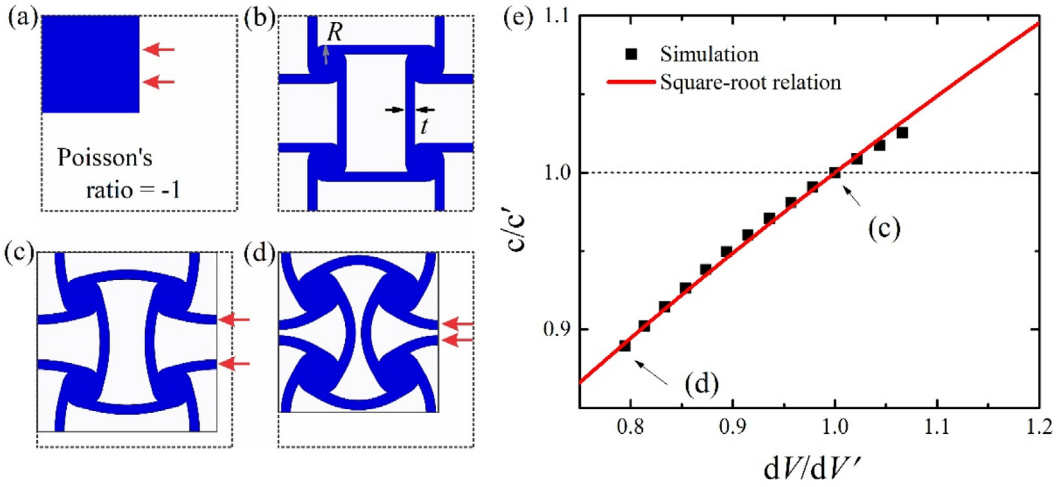

Fig. 1. Requirement of quasi-conformal mapping. Schematics of isotropic deformation (a) with Poisson's ratio of −1, and anti-tetrachiral structures under (b) 0, (c) 8% and (d) 18% compression strain. Here, the length (L) of the unit cell is taken as 20 mm, and the circle diameter (R) and wall thickness (t) inside the cell are 2 mm and 1 mm, respectively. (e) The graph shows the square-root relation between the effective sound speed variation (c/c') and the unit cell volume change (dV/dV'). Dots: data obtained by Comsol simulation. Line: theoretical prediction.

from the virtual space (with primed parameters) are given by [22]

$$\rho = J(\mathbf{A}^T)^{-1}\rho'(\mathbf{A}^{-1}),$$
$$\kappa = \kappa' J \tag{1}$$

where $\mathbf{A}$ is the Jacobian matrix of the transformation, and $J = \det(\mathbf{A})$ is the determinate, indicating the volumetric change at a voxel, that is, $J = dV/dV'$. In particular for conformal mapping, it gives $\mathbf{A}\cdot\mathbf{A}^{\mathrm{T}}/J = 1$ [23]. By assuming uniformly distributed material density (ρ') and bulk modulus (κ') in the virtual space, Eq. (1) leads to

$$\rho = \rho',$$
$$\kappa = \kappa' J. \tag{2}$$

Eq. (2) shows that the density distribution in the physical space induced by conformal mapping is still uniform and equal to that in the virtual space while the bulk modulus changes by a factor of J. Moreover, with constant density, the effective sound speed distribution exhibits a square-root dependence on the volumetric change of the medium according to Eq. (2), that is,

$$c/c' = \sqrt{dV/dV'} = \sqrt{J}. \tag{3}$$

Thus, Eq. (2) (or Eq. (3)) depicts the acoustic material property distribution that needs to be fulfilled by the structure deformation.

With known the requirement of quasi-conformal mapping, we probe suitable matrix materials and lattice structures to realize the self-adaptive acoustic cloak. Actually, the isotropic prerequisite is coincident with the deformation pattern of lattice structures with Poisson's ratio of −1, which maintains the structure isotropy even under compression or tension (Fig. 1a). Structures like anti-tetrachiral honeycombs that can be achieved by 3D printing or template molding have been shown to exhibit a "-1" Poisson's ratio over a large range of deformation [24], as illustrated in Fig. 1b–d. Regarding the material system, such a cloak design can hardly be realized in air as air already has the almost minimum bulk modulus while Eq. (2) requires even more reduced bulk modulus than that of the background. Instead, a tiny amount of air bubbles in water significantly decreases the water bulk modulus but negligibly affects the effective density. This implies the feasibility of constructing the designed acoustic cloak in water. In order to well control the position of those air bubbles, a solid matrix with water-like acoustic properties can be used as a host. For example, silicone elastomer (or PDMS) has a similar density with water and has also been demonstrated to be able to well match the acoustic impedance of water in a wide frequency range [21]. Thus, by using such a water-like acoustic material as matrix, the further adding of a small volume fraction of air bubbles through micro-injection or emulsion templating techniques can enable the efficient modulation of the effective bulk modulus and thus the effective sound speed [25,26].

The effective density and modulus of a composite lattice structure in water can be estimated by a weighted average of those from all the components [5],

$$\rho = (1-f_g)\rho_{\mathrm{w}} + f_g\rho_g \approx \rho_{\mathrm{w}},$$
$$\kappa^{-1} = (1-f_g)\kappa_w^{-1} + f_g\kappa_g^{-1} \approx f_g\kappa_g^{-1} \tag{4}$$

where ρ_{w} and κ_{w} are density and bulk modulus of water or water-like matrix material, ρ_{g} and κ_{g} are density and bulk modulus of air, and f_g is volume fraction of the air. The approximations on the right hand side of Eq. (4) are taken by considering $f_g << 1$, $\rho_{\mathrm{g}} << \rho_{\mathrm{w}}$, and $\kappa_{\mathrm{g}} << \kappa_{\mathrm{w}}$. As the total amount of air in the matrix is fixed, a volume change by a factor of J in the system leads to the air fraction in a deformed state (corresponding to the physical space in the coordinate transformation) obtained as

$$f_g = f_g' J^{-1} \tag{5}$$

where f_g' is the air fraction in the reference state (corresponding to the virtual space in the coordinate transformation). The combination of Eqs. (4) and (5) directly leads to Eq. (2), hinting the automatic satisfaction of the requirement of quasi-conformal mapping by elastically deforming lattice structures with Poisson's ratio of −1 and made of water-like acoustic materials.

With an eye on estimating how well the quasi-conformal mapping requirement is fulfilled by the lattice structure deformation, we employ acoustic simulation combined with solid structure deformation using Comsol Multiphysics to probe the effective sound speed variation with the volume change for a unit anti-tetrachiral cell in a background of water. Since the matrix material is based on silicone elastomer, the whole structure is highly flexible. Moreover, instead of directly simulating air bubbles distributed in the water-like matrix, we consider the porous matrix as an effective medium with similar density with water but

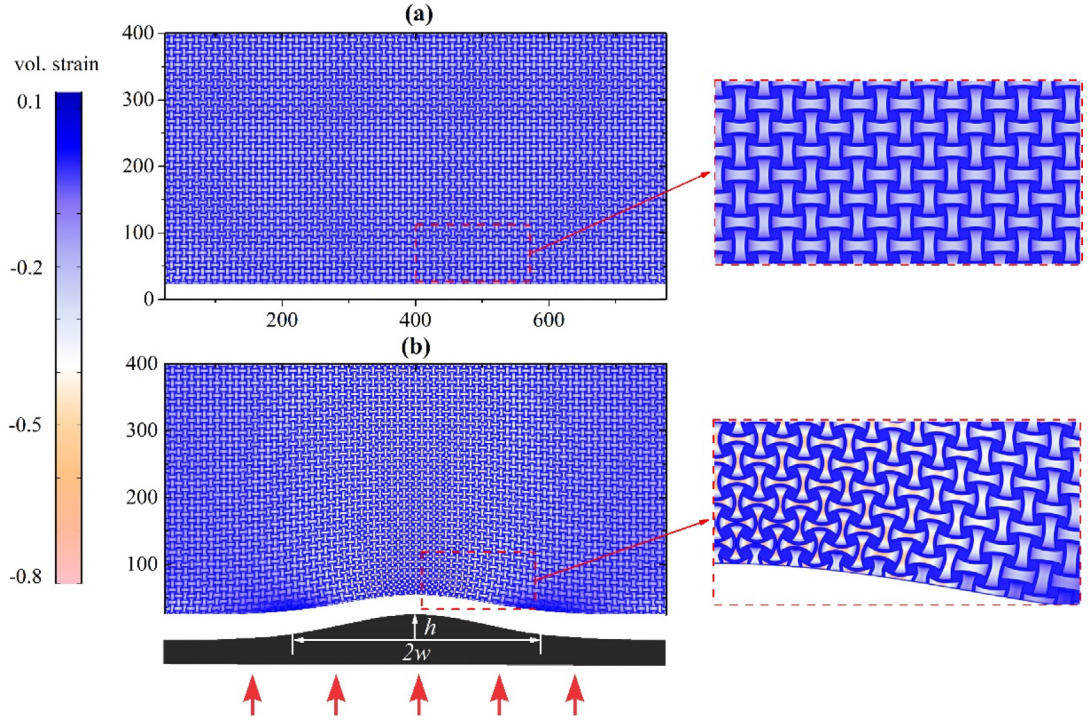

Fig. 2. Self-adaptive acoustic cloak enabled by structure deformation. (a) and (b) show the initial and deformed states of the designed acoustic cloak, respectively. Color bar indicates the relative magnitude of volume strain. Insets show the zoom-in regions in the red dashed boxes. In (b), the bump profile is described by $h{\cdot}\exp[-(x-x_c)^2/w^2]$, where h (= 20 mm) is bump height, x_c is x coordinate at the center, and $2w$ (= 300 mm) is bump width. The maximum bump height is limited by the deformation capability of the anti-tetrachiral structure, the walls of which tend to touch with each other under more vigorous deformation or get overstretched beyond the isotropic deformation regime.

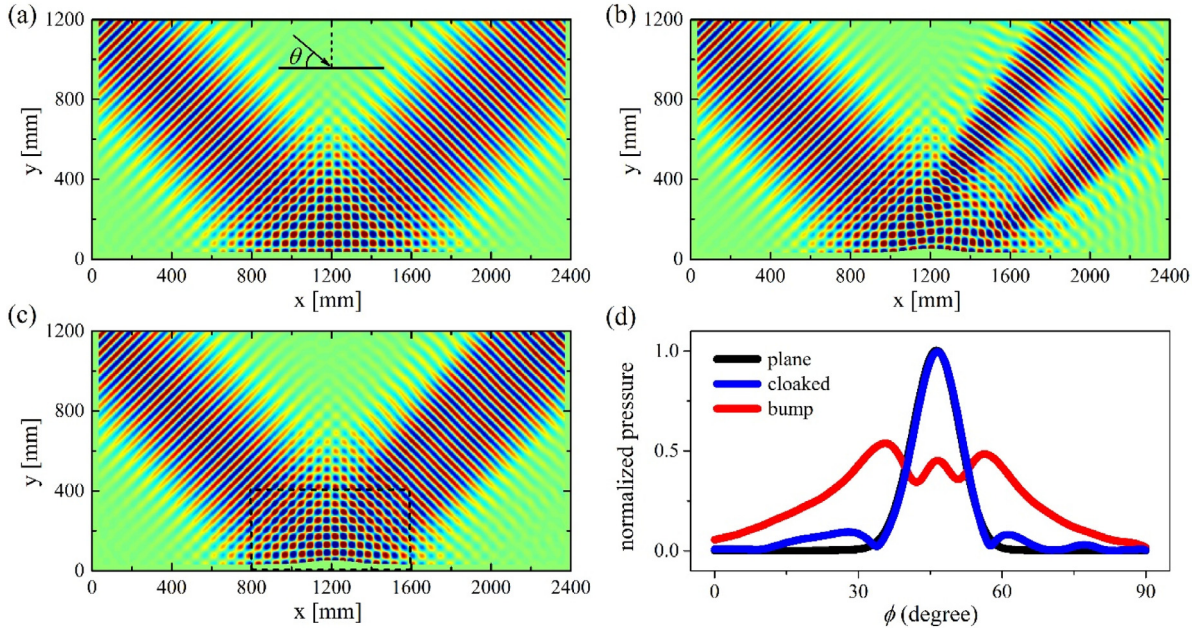

Fig. 3. Near-field and far-field acoustic pressure distribution. Near-field wave patterns are obtained with a Gaussian beam incident at 45 degree on (a) a ground plane, (b) rigid bump, and (c) cloaked rigid bump. Inset in (a) shows the definition of the incident angle (θ). The black dashed box in (c) shows the position of the designed cloak. The bump height, $h = 20$ mm, and the bump width, $2w = 300$ mm. (d) The graph shows the corresponding far-field patterns of the above three cases.

reduced effective sound speed (c_m, e.g., equal to 0.45 c_w, corresponding to an air volume fraction below 1% [25]. Here, c_w is sound speed of water). Indeed, the effective sound speed of the unit cell perfectly follows the square-root relation with the volume change in a wide range of deformation (Fig. 1e). The use of a slightly compressed configuration (e.g., under 8% compression strain, see Fig. 1c) as the reference state is based on the consideration that the lattice structures needs the ability to experience both compression and tensile strains while still maintaining the Poisson's ratio of -1 to satisfy the need of cloak design. Moreover, the similar satisfaction of the cloak design requirement by deforming an anti-tetrachiral unit cell distributed with air bubbles

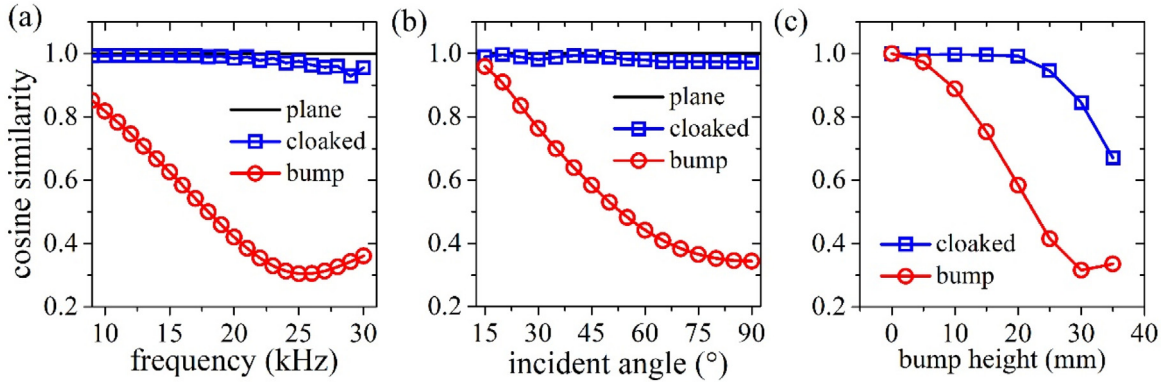

Fig. 4. Cosine similarity of far-field patterns. The graphs show the cosine similarity variation as a function of frequency (a), incident angle (b), and bump height (c) for bare rigid bump and cloaked rigid bump, respectively. Those values are referenced to that of the ground plane (i.e., '1'). In (a), the incident angle is 45 degree, and the bump height is 20 mm. In (b), the frequency is 16 kHz, and the bump height is 20 mm. In (c), the frequency is 16 kHz, and the incident angle 45 degree. The bump width (see Fig. 2b) is kept constant at $2w = 300$ mm in all three cases.

verifies the rationality of the current effective medium approach (see fig. S1b in Supplementary Materials). In addition, it is found that the acoustic absorption due to the presence of air bubbles of very tiny size and low volume fraction in the matrix is rather weak in the current frequency range of interest and, thus, will not be considered in the acoustic simulation below (see fig. S1d in Supplementary Materials).

From above, it is seen that the elastic deformation of an anti-tetrachiral unit cell manages to satisfy both the material isotropy and acoustic property distribution requirements of quasi-conformal mapping. Then, we attempt to build up an acoustic carpet cloak by using a periodic lattice structure of the anti-tetrachiral cells (e.g., with a length of 20 mm). The initial reference state (Fig. 2a), corresponding to the virtual space in the coordinate transformation, is constructed by those unit cells under a strain of 8% (Fig. 1c) for the ability to sustain both compression and tensile strains without derivation from the isotropic deformation. When pressed on a rigid bump with height (h) and width ($2w$), the whole lattice structure is expected to transform and get self-adapted according to the quasi-conformal mapping. The real deformation of the lattice structure obtained by the simulation indeed shows typical characteristics of the transformed physical space induced by quasi-conformal mapping (Fig. 2b). The lattice cells experience concentrated compression around the top of the bump and slight stretching near the bump edges since the top and side boundaries of the lattice structure are fixed.

To examine the performance of such a designed acoustic cloak, we carry out acoustic simulation and compare the near-field and far-field wave patterns when a Gaussian beam is incident on a ground plane, rigid bump, and cloaked rigid bump from an angle of 45 degree, respectively. Compared to the ground plane (Fig. 3a), the reflected beam on the rigid bump is clearly perturbed and scattered (e.g., at a frequency of 16 kHz) (Fig. 3b). When the designed flexible lattice structure is pressed on the rigid bump, the reflected beam emerges as a single one again (Fig. 3c), indicating an acoustic carpet cloak has been realized by elastically deforming the lattice structure. The far-field pattern with a single pronounced peak on the cloaked rigid bump similar to that on a ground plane also demonstrates the good cloaking performance (Fig. 3d). Instead, the far-field pattern on the rigid bump shows multiple pronounced peaks.

We also quantify the performance of the designed acoustic cloak using the cosine similarity of far-field patterns (see Fig. 3d) at difference frequency, incident angle, and bump height. The cosine similarity (CS) is expressed by [27]

$$CS = \frac{\mathbf{p}^r \cdot \mathbf{p}^0}{|\mathbf{p}^r|\,|\mathbf{p}^0|} = -\frac{\sum_{i=1}^{n} p_i^r \times p_i^0}{\sqrt{\sum_{i=1}^{n}\left(p_i^r\right)^2} \times \sqrt{\sum_{i=1}^{n}\left(p_i^0\right)^2}}, \tag{6}$$

where $\mathbf{p}^r$ is the pressure field for the ground plane (as reference values) and $\mathbf{p}^0$ is the pressure field for the bare or cloaked rigid bump. The close cosine similarity for the cloaked rigid bump to that for the ground plane (i.e., '1') in a large range of frequency and incident angle manifests the broadband characteristic of the acoustic cloak (Fig. 4a and b). This is in consistence with typical metamaterials designed by quasi-conformal mapping [28]. In contrast, large derivation from '1' is observed for the far-field pattern from the rigid bump, especially at high frequency and high incident angle. Moreover, the self-adaptive characteristic of the designed cloak allows the bump to have varied height, which is proved by the good cloaking performance when the bump height is below 20 mm (Fig. 4c). However, the cloaking effect deteriorates with the further increase of the bump height, indicating a limitation originating from the deformation capability of the lattice cells. It is due to the fact that extreme compression or stretching of those lattice cells could cause the deformation to significantly deviate from the isotropic behavior and thus the failure to satisfy the requirement of quasi-conformal mapping any more. This definitely deserves extra future efforts for a better design of those auxetic structures.

In summary, we have designed a self-adaptive and broadband acoustic cloak in both frequency and incident angle, which is automatically formed by elastically deforming a flexible lattice structure with Poisson's ratio of -1. The deformation spontaneously fulfills the requirement of the quasi-conformal mapping, that is, the material isotropy and square-root sound speed distribution with the volumetric change. The finding here, which is ready to be extended into the 3D case [29], enables a convenient way to construct acoustic metamaterials without the necessity to design the whole structure through a point-by-point method. Although the currently design cloak appears bulky as limited by the deformation capability of the anti-tetrachiral structure, with the emerging of more advanced mechanical metamaterials, it is envisioned that different kinds of novel acoustic metamaterials targeted for various engineering applications can be quested based on the concept developed here.

Declaration of competing interest

The authors declare that they have no known competing financial interests or personal relationships that could have appeared to influence the work reported in this paper.

Acknowledgement

This work is supported by the Ernest S. Kuh Endowed Chair Professorship.

Appendix A. Supplementary data

Supplementary material related to this article can be found online at https://doi.org/10.1016/j.eml.2021.101347.

References

[1] G. Ma, P. Sheng, Sci. Adv. 2 (2016) e1501595.
[2] S.A. Cummer, J. Christensen, A. Alù, Nat. Rev. Mater. 1 (2016) 16001.
[3] J. Zhu, J. Christensen, J. Jung, L. Martin-Moreno, X. Yin, L. Fok, X. Zhang, F.J. Garcia-Vidal, Nat. Phys. 7 (2010) 52–55.
[4] H. Chen, C.T. Chan, J. Phys. D: Appl. Phys. 43 (2010) 113001.
[5] R.V. Craster, S. Guenneau, Acoustic Metamaterials: Negative Refraction, Imaging, Lensing and Cloaking, Springer Science & Business Media, 2012.
[6] Z.Y. Liu, X.X. Zhang, Y.W. Mao, Y.Y. Zhu, Z.Y. Yang, C.T. Chan, P. Sheng, Science 289 (2000) 1734–1736.
[7] N. Fang, D. Xi, J. Xu, M. Ambati, W. Srituravanich, C. Sun, X. Zhang, Nature Mater. 5 (2006) 452–456.
[8] J.S. Li, J.B. Pendry, Phys. Rev. Lett. 101 (2008).
[9] M. Gharghi, C. Gladden, T. Zentgraf, Y.M. Liu, X.B. Yin, J. Valentine, X. Zhang, Nano Lett. 11 (2011) 2825–2828.
[10] W.R. Zhu, C.L. Ding, X.P. Zhao, Appl. Phys. Lett. 97 (2010).
[11] B.I. Popa, S.A. Cummer, Phys. Rev. B 83 (2011).
[12] K. Bertoldi, V. Vitelli, J. Christensen, M. van Hecke, Nat. Rev. Mater. 2 (2017).
[13] K.H. Yu, N.X. Fang, G.L. Huang, Q.M. Wang, Adv. Mater. 30 (2018).
[14] D. Shin, J. Kim, C. Kim, K. Bae, S. Baek, G. Kang, Y. Urzhumov, D.R. Smith, K. Kim, Nature Commun. 8 (2017).
[15] Y. Zarate, S. Babaee, S.H. Kang, D.N. Neshev, I.V. Shadrivov, K. Bertoldi, D.A. Powell, Sci. Rep. 6 (2016).
[16] N. Gao, J. Li, R.H. Bao, W.Q. Chen, Soft Matter 15 (2019) 2921–2927.
[17] C.M. Portela, A. Vidyasagar, S. Krodel, T. Weissenbach, D.W. Yee, J.R. Greer, D.M. Kochmann, Proc. Natl. Acad. Sci. USA 117 (2020) 5686–5693.
[18] L. Jin, R. Khajehtourian, J. Mueller, A. Rafsanjani, V. Tournat, K. Bertoldi, D.M. Kochmann, Proc. Natl. Acad. Sci. USA 117 (2020) 2319–2325.
[19] D. Shin, Y. Urzhumov, Y. Jung, G. Kang, S. Baek, M. Choi, H. Park, K. Kim, D.R. Smith, Nature Commun. 3 (2012).
[20] D. Shin, Y. Urzhumov, D. Lim, K. Kim, D.R. Smith, Sci. Rep. 4 (2014).
[21] R.M. Guillermic, M. Lanoy, A. Strybulevych, J.H. Page, Ultrasonics 94 (2019) 152–157.
[22] J.B. Pendry, J. Li, New J. Phys. 10 (2008).
[23] L. Xu, H. Chen, Nat. Photonics 9 (2014) 15–23.
[24] A. Alderson, K.L. Alderson, D. Attard, K.E. Evans, R. Gatt, J.N. Grima, W. Miller, N. Ravirala, C.W. Smith, K. Zied, Compos. Sci. Technol. 70 (2010) 1042–1048.
[25] K. Zimny, A. Merlin, A. Ba, C. Aristegui, T. Brunet, O. Mondain-Monval, Langmuir 31 (2015) 3215–3221.
[26] K. Zhang, C. Ma, Q. He, S.T. Lin, Y. Chen, Y. Zhang, N.X. Fang, X.H. Zhao, Adv. Funct. Mater. 29 (2019).
[27] J. Zhu, T.N. Chen, Q.X. Liang, X.P. Wang, J. Xiong, P. Jiang, J. Phys. D: Appl. Phys. 48 (2015).
[28] R. Liu, C. Ji, J.J. Mock, J.Y. Chin, T.J. Cui, D.R. Smith, Science 323 (2009) 366–369.
[29] D. Shin, J. Kim, D.S. Yoo, K. Kim, Opt. Express 23 (2015) 21892–21898.